Stony Brook University

Light-induced Self-assembly and Diffusion of Nanoclusters

A Thesis Presented

by

Wenxuan Lian

to

The Graduate School

in Partial Fulfillment of the

Requirements

for the Degree of

Master of Science

in

Materials Science and Engineering

Stony Brook University

December 2016

Stony Brook University

The Graduate School

Wenxuan Lian

We, the thesis committee for the above candidate for the

Master of Science degree, hereby recommend

acceptance of this thesis.

Dr. Oleg Gang – Thesis Advisor
Group Leader for Soft and Bionanomaterial Group
Center for Functional Nanomaterials
Brookhaven National Laboratory

Dr. Yizhi Meng – Second Reader
Assistant Professor
Materials Science and Chemical Engineering
Stony Brook University

Dr. Tadanori Koga – Third Reader
Associate Professor
Materials Science and Chemical Engineering
Stony Brook University

This thesis is accepted by the Graduate School

Charles Taber
Interim Dean of the Graduate School

Abstract of the Thesis

Light-induced Self-assembly and Diffusion of Nanoclusters

by

Wenxuan Lian

Master of Science

in

Materials Science and Chemical Engineering

Stony Brook University

2016

Novel methods to build multiple types of three-dimensional structures from various nanoscale components are the most exciting and challenging questions in nano-science. The properties of the assembled structures can be potentially and designed, but the development of such approaches is challenging. In order to realize such rational assembly, a tunable interaction medium is often introduced into the system. Soft matter, such as polymers, surfactants and biomolecules are used to modify the surfaces of the nanoscale building blocks. Deoxyribonucleic acid (DNA) strands are known as polynucleotides since they are composed of simpler units called nucleotides. There are unique base pairing rules that are predictable and programmable, which can be used to regulate self-assembly process with high degree of control. Besides controlling static structure, it is important to develop methods for controlling systems in dynamic matter, with chemical stimuli or external fields. For example, here we study the use of azobezene-trimethylammonium bromide (AzoTAB) as a molecular agent that can control self-assembly via light excitation. In this thesis, DNA assisted self-assembly was conducted. The ability of AzoTAB as a light induced surfactant to control DNA assisted self-assembly was confirmed. The mechanism of AzoTAB as a light controlled self-assembly promoter was studied. In the second project, diffusion of nanoclusters was studied. The presence of polymers brings strong entanglement with

nanoclusters. This entanglement is more obvious when the nanocluster is a framed structure like the octahedron in the study. The diffusion coefficient of the octahedron becomes larger during traveling. The following up studies are required to elucidate the origin of the observed effect.

Dedication

I would like to dedicate this thesis to my grandfather, who was a great architect. Cancer has taken him from me, but I shall always remember the joy on his face when he knew about me doing research on nanomaterials.

Acknowledgement

I would like to express my sincere gratitude to all the lab members from Dr. Oleg Gang's group at Center for Functional Nanomaterials.

Dr. Ye Tian, Dr. Wenyan Liu, Dr. Fang Lu, and Dr. Yugang Zhang helped me with some experimental problems during my research.

My dear parents and husband, Xiuping Zan, are very supportive. They give me courage and hope.

Table of Contents

List of Figures

List of Equations

1 Introduction

1.1 General Introduction of Self-assembly

Novel methods to build multiple types of three-dimensional structures from various nanoscale components, or "nanoscale building blocks", are the most exciting and challenging questions in nano-science. Unlike other approaches such as lithography, which has limited abilities to control nanostructure with wet chemistry methods, self-assembly is a promising and controllable way to fabricate new nanomaterials. However, the strategies of developing more refined and tunable structures have not yet been well-established.

Just like how atoms bind together to form larger scale structures, nanoscale components can be assembled into different structures. The properties of the assembled structures can be predicted and designed. In order to realize this kind of tunable assembly, an interaction medium is introduced into the system. Soft matter, such as polymers, surfactants and biomolecules are used to modify the surfaces of the nanoscale building block [1]. The soft matter medium provides a strong binding force and offer flexible spacers among the building blocks. If one compares hard-core nanoscale components as the bricks in the architecture, soft matter will serve as the cement but better than the cement because soft matter not only hold the "bricks" together, but also can be programmed to make more complex structures. Various biological interactions, such as DNA hybridization and protein recognition, provide a programmable approach to novel structures [2].

1.2 DNA in Self-assembly

1.2.1 Brief Introduction of DNA

Deoxyribonucleic acid (DNA) is a molecule that encodes the genetic information in all known living organisms. Most DNA molecules consist of two biopolymer strands coiled around each other to form a double helix. The diameter of the helix is around 2nm. The length of a base pair is 0.34nm. Ten base pairs compose of one helical turn, which has the length of 3.4nm. The two DNA strands are known as polynucleotides since they are composed of simpler units called nucleotides. Each nucleotide is composed of a nitrogen-containing nucleobase: guanine (G), adenine (A), thymine (T), or cytosine (C), as well as a monosaccharide sugar called deoxyribose and a phosphate group. The nucleotides are joined to one another in a chain by covalent bonds between the sugar of one nucleotide and the phosphate of the next, resulting in an alternating sugar-phosphate backbone. According to base pairing rules (A with T and C with G), hydrogen bonds bind the nitrogenous bases of the two separate polynucleotide strands to make double-stranded DNA. These unique base pairing rules are predictable and programmable, which can be used to regulate self-assembly process.

Using DNA as a medium for self-assembly in nanotechnology was proposed around 30 years ago [3]. A great strategy to control DNA-DNA connection is through “sticky ends”. Sticky ends are complementary single-stranded DNA tips that will hybridize and therefore joint two DNA molecules together [4].

1.2.2 DNA Origami

A new approach of building 2-dimensional patterns from DNA molecules were reported by Rothermund in the year 2006 [5]. A DNA origami is basically a 2-dimensional DNA pattern formed by a large number of short single-stranded DNA molecules connected onto a long scaffold DNA molecule. M13mp18 genomic DNA (M13) is a commonly used scaffold that can be folded into different shapes with the assistant of different short complementary DNA called staple strands. Figure 1-1 shows some examples of

different DNA origami patterns. DNA origami can be formed by a single-step mixing and annealing [5] [6] [7] [8] [9] [10] [11] [12] .

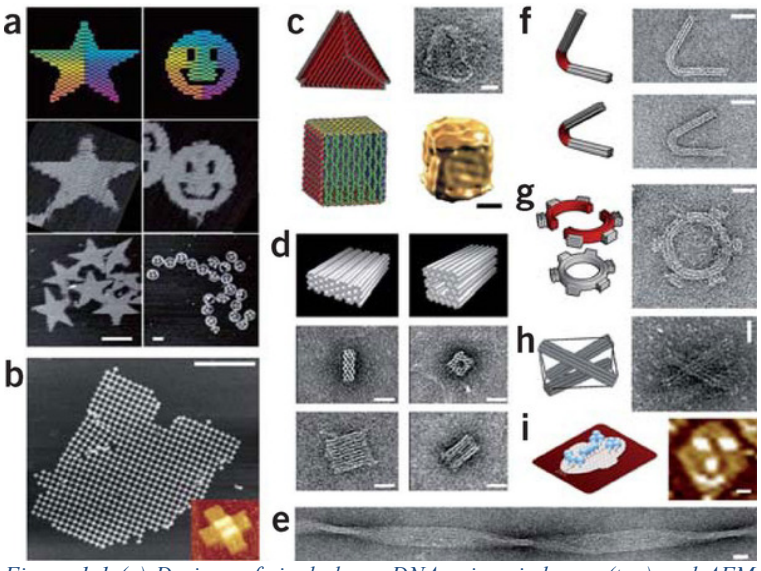

Figure 1-1 (a) Designs of single-layer DNA origami shapes (top) and AFM images of these objects (middle and bottom). The pointed star and the smiley face each have diameters of ~100 nm. (b) AFM image of crystalline DNA origami arrays formed from several hundred copies of a cross-shaped single-layer DNA origami object. Inset, image of a 100-nm-long cross-shaped origami monomer. (c) Container-like DNA origami objects (left) imaged with negative-stain TEM (top) and cryogenic TEM (bottom) (d) Design and images of multilayer DNA origami objects. (e) Image of a multimeric multilayer DNA origami object with global twist deformation. (f,g) Design and images of space-filling multilayer DNA origami objects such as bent bars (f) and a gear with square teeth (g) displaying custom curvature. (h) Tensegrity prism created by combining multilayer DNA origami struts and ssDNA strings; reprinted. (i) Design and image of a single-layer DNA origami shape with site-directed protein attachments; Scale bars, 100 nm (a), 1,000 nm (b) and 20 nm (c–i).

1.2.3 Functionalization of Nanoparticles with DNA Oligonucleotides

To utilize the hybridization of complementary single-stranded DNA molecules as a self-assembly medium, the nanoscale components need to be capped with a shell of DNA molecules. This process is called functionalization. In my studies, the nanoscale components are gold nanoparticles (AuNPs). The sizes of AuNPs used in my studies vary from 5nm to 50nm. Around 20 years ago, it was reported that some polymers could be attached to the surface of nanoparticles by covalent bonds [13] . Mirkin *et al.* reported a successful functionalization of AuNPs with DNA oligonucleotides [14]. After that exciting success, a general strategy was developed. It was reported that the number of oligonucleotides attached on

the particle surface can be tuned by varying the ratio of AuNP and DNA, the salt aging concentration and the size of the AuNP.

Recently, not only the spherical nanoparticles were reported to be functionalized by DNA oligonucleotides, carbon nanotubes and quantum dots were also reported as substrates [15] [16] [17].

1.2.4 DNA Assisted Self-assembly

Systematical studies have been done about the thermodynamic and kinetic process of DNA assisted self-assembly. To calculate the interaction free energy between two DNA functionalized colloidal nanoparticles, two contributions need to be taken account of: the attraction caused by the hybridization of the two single-stranded DNA oligonucleotides and the repulsion between two shells of DNA brushes on the particles [18] . One of the merits of DNA assisted self-assembly, which was mentioned several times in this proposal, is the programmability of the system. That is, the attraction and repulsion contributions can be tuned quantitatively. For example, the attraction can be tuned simply by varying the base number of the sticky ends of the single-stranded DNA oligonucleotides; the steric repulsion between DNA brushes can be calculated by finding the probability of their connected configuration in a confined environment using a statistical mechanics. According to free energy function $\Delta G=\Delta H-\Delta ST$, it is very easy to see that temperature T has very significant impact on the phase behavior of DNA functionalized nanoparticles. More details can be found in references [19] [20] [21] [22] [23] [24] .

Experimentally, two critical challenges need to be noticed in DNA assisted self-assembly. First, the attraction brought by the complementary single-stranded DNA oligonucleotides is strong enough to trap the system in metastable free-energy minima. This trap can slow down the equilibration of the system. One way to avoid this slow-down is to reduce the attraction by introducing inert/neutral polymers of DNA strands. There is a limit in the grafting sites on each nanoparticle, therefore the density of active DNA strands decreases. Second, DNA assisted self-assembly systems are very sensitive to temperature

changes. The melting temperature of DNA strands in aggregations can be much higher than the melting temperature of the same DNA strands due to multiple linkages [25].

1.3 Diffusion of Nanoclusters

Robert Brown observed a fast and erratic motion of small particles through microscope in the year 1827. Since that time, the study of the meso-scale diffusion emerged. Brownian motion is the random motion of particles moving freely in a liquid or a gas. This motion results from the collision with the quick atoms or molecules in the gas or liquid. Years later, Einstein and Von Smolchowski worked on the quantitative description of Brown motion. With the help of their theory, Jean Perrin provided the first direct evidence of the existence of molecules and an estimated value of Avogadro's number.

The driving force of normal diffusion (with the absence of any external field) is the gradient of chemical potential. For a one-dimensional diffusion, the driving force is the function of chemical potential (μ_i) and displacement x,

$$F_d = -\frac{d\mu_i}{dx} \qquad \textit{Equation 1-1}$$

Divided by the total number of particles, the diffusion force per particle is:

$$f_d = -\frac{(\frac{kT}{c_i})dc_i}{dx} \qquad \textit{Equation 1-2}$$

where c_i is the concentration.

On the other hand, the viscous force, which is opposite to the driving force, can be described as:

$$f_v = Bu \qquad \textit{Equation 1-3}$$

where B is the friction coefficient, and u is the travel speed of the particle.

Fick's first law gives the relationship between the flux and concentration as follows:

$$J_i = u_d c_i = -D\frac{dc_i}{dx} \qquad \textit{Equation 1-4}$$

where u_d is the terminal speed when the driving force equals to the viscous force $f_d=f_v$, and D is diffusion coefficient.

Then we will get the Stokes-Einstein equation:

$$D = \frac{kT}{B} = \frac{kT}{6\pi\eta r} \qquad \textit{Equation 1-5}$$

where $B=6\pi\eta r$ for spherical particle of radius r.

Experimentally, the measurement of the diffusion coefficient D starts with the records of the mean square displacement (MSD, denoted as $<x^2>$) of each particle as a function of time t:

$$< x^2 >= \frac{\int_{-\infty}^{\infty} x^2 c(x,t) dx}{\int_{-\infty}^{\infty} c(x,t) dx} \qquad \textit{Equation 1-6}$$

The mean square displacement is also related to diffusion coefficient D:

$$< x^2 >= 2Dt \qquad \textit{Equation 1-7}$$

where 2 is the dimensional constant for one-dimension, while 4 and 6 are for two and three-dimension respectively.

However, not all diffusions can be described by Einstein's equation. Therefore, a universal equation is as follows:

$$< x^2 >= q_i D t^{\alpha} \qquad \textit{Equation 1-8}$$

where q_i is the dimensional constant mentioned before (2,3, and 4 are for 1, 2, and 3-dimension), and α is a constant that describe the diffusion type. When $\alpha<1$, the diffusion type is called sub-diffusion. It is common in particle diffusing in entangled polymer environments; when $\alpha>1$, the diffusion type is called super-diffusion. It occurs with the presence of external forces.

1.4 Characterization Methods

1.4.1 Dynamic Light Scattering (DLS)

Dynamic light scattering (DLS) offers a simple way to probe the diffusion of particles in solution. Despite its easy setup, DLS results contain rich information collected from numerous particles that can analyze particle size distribution as well as parameters of the solution such as viscosity.

In a DLS setup, a monochromatic laser is shot through a polarizer into a solution sample. All the particles in the solution sample scatter the light and the scattered light is collected by a detector at a certain angle. Due to the fast Brownian motion of each particle in the solution, the intensity of the scattered light fluctuates with time. This scattered light then undergoes either constructive or destructive interference by the surrounding particles, and within this intensity fluctuation, information is contained about the time scale of movement of the scatterers. This fluctuation can be described by an autocorrelation function,

$$I(q,t) \equiv \langle I(q,t_0)I(q,t+t_0)\rangle \qquad \textit{Equation 1-9}$$

where < > denotes the ensemble average of the intensity, and I(q,t) is the instantaneous intensity.

The first-order autocorrelation function describes the movement of correlated particles,

$$G_1 = \frac{1}{T}\int_0^T E(t)E(T+\tau)d\tau \qquad \textit{Equation 1-10}$$

The second-order autocorrelation function describes the intensity change of scattered light,

$$G_2(\tau) = \frac{1}{T}\int_0^T I(t)I(T+\tau)d\tau \qquad \textit{Equation 1-11}$$

The relationship between the two auto-correlation functions can be described by Siegert equation,

$$G_2(\tau) = B[1 + \beta G_1(\tau)^2] \qquad \textit{Equation 1-12}$$

where G is the baseline and β is an instrumental parameter, both of which are constants.

Once the autocorrelation data have been generated, different mathematical approaches can be employed to determine the information from it. The simplest approach is to treat the first order autocorrelation function as a single exponential decay,

$G_1(\tau) = e^{-\Gamma\tau}$ *Equation 1-13*

where Γ is the decay rate $\Gamma = q^2 D$, where D is the diffusion coefficient of the particles in solution and is often used to calculate the hydrodynamic radius of a sphere through the Stokes–Einstein equation,

$D = \frac{kT}{3\pi\eta d_h}$ *Equation 1-14*

where η is the viscosity of the solution and r is the hydrodynamic radius of the particle.

1.4.2 Small Angle X-ray Scattering (SAXS)

Small angle scattering is a technique that the elastic scattered light is recorded at a very low angular range (0.1-10°). In this angular range, information about the shape and size of macromolecules, characteristic distances of partially ordered materials, pore sizes can be probed. The sample can be a crystal or a dilute solution. In my study, I mainly worked on dilute systems.

The incident monochromatic X-ray of wavelength λ is shot through the sample. Some of the light can pass through and remain intact, while other light is scattered from the particle at an angle ϑ and interfere with each other. This interference carries the information of the structure of the sample and then falls onto the detector, which is typically a 2-dimensional flat screen located at the back of the sample. The detector records the intensity of the scattered light.

If the scattering is not strong enough to incident multiple scattering, the scattered intensity I(q) can be described as

$I(q) = |A(q)|^2 = \left|\int \rho(r) e^{-i2\pi sr} dr\right|^2$ *Equation 1-15*

where q is the scattering vector, A is the amplitude of the scattering, and ρ(r) is the scattering length density distribution. The scattering vector q can be described by

$q \equiv 2\pi s = \left(\frac{4\pi}{\lambda}\right) sin\frac{\vartheta}{2}$ *Equation 1-16*

where the unit of q is length $^{-1}$ and therefore q spans a three-dimensional reciprocal space. While the structural information of the sample is contained in the function ρ(r) over the entire sample volume (integrity over all r values) in real space, the Fourier transform of ρ(r), the amplitude A(q) is over the entire q in the reciprocal space. This relationship between ρ(r) and A(q) can be described by the inverse Fourier transform

$\rho(r) = \int A(q)e^{iqr}\, dq$ ***or*** $\rho(r) = \int A(s)e^{i2\pi sr} ds$ *Equation 1-17*

Therefore, ρ(r) and A(q) are actually equivalent to each other. The structural information of the sample is delivered.

2 Light Induced Self-assembly with AzoTAB

2.1 Introduction

2.1.1 Photoisomerization and Photoisomers

Electrons travel in different energy levels in atoms. Once an electron gains energy, which can be done by absorbing energy from photon, the electron will move to a higher energy state. This process is called photoexcitation (PE). If an incident photon can eject one or more electrons from an atom, photoionization occurs. When the energy of the photon is too low to cause photoionization, the absorption of the photon takes place in accordance with Planck's quantum theory.

In chemistry, a molecule is an electrically neutral group of two or more atoms held together by chemical bonds. Due to the properties of chemical bonds, molecules usually exist in unique structures. When the structure of a molecule changes between its isomers resulting from photoexcitation, this molecular behavior is called photoisomerization. Both reversible and irreversible photoisomerization reactions exist.

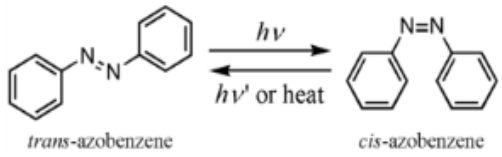

Figure 2-1 The photoisomerization of azobenzene

A widely used example of photoisomer is azobenzene. Azobenzene is an important and simplest member among the azo compounds, which bear the functional group R-N=N-R'. In an azobenzene molecule, R and R' are both phenyl rings. The photoisomer used in my studies, azoTAB, is a derivative of azobenzene. The most interesting property of azobenzene is the photoisomerization of *trans* and *cis* isomers. The photoisomerization is a rapid process of 10-12 s time scale. Ultraviolet (UV) light, which corresponds to the energy gap of the π-π* (S2 state) transition, can switch *trans* isomers to *cis*. For *cis*-to-*trans* conversion, blue light, which is equivalent to that of the n-π* (S1 state) transition, is the switch. For a variety of reasons, the *cis* isomer is less stable than the *trans* isomer. Thus, *cis*-azobenzene will thermally

relax back to the *trans* state via *cis*-to-*trans* isomerization. Figure 2-1 shows the photoisomerization of azobenzene.

The mechanism of azobenzene photoisomerization is still under debate in literature. Two modes of conversion, inversion and rotation, were proposed. Inversion happens when the two nitrogen atoms and phenyl groups remain in the same plane during photoisomerization, while rotation occurs when one of the nitrogen atoms rotate to another plane [26].

2.1.2 Properties of AzoTAB surfactant

Azobezene-trimethylammonium bromide surfactant (AzoTAB) is a derivative of azobenzene. AzoTAB is composed of four main parts: a trimethylammonium head group providing the hydrophilic part of the surfactant, a hydrophobic tail composed of a spacer alkyl group between the head group and the azobenzene moiety, a photoresponsive azobenzene group, and an alkyl tail group. The presence of the double bond and the sp^2 hybridization of the nitrogen impose the molecule to be planar. The *cis* isomer of AzoTAB however has been shown to deviate from the planar configuration and adopt a distorted conformation due to steric interactions between the ortho hydrogen of the benzene rings. Azobenzene compounds are known to exhibit *trans-cis* isomerization induced by photo-illumination. As shown in Figure 2-2, when kept in the dark or blue light (430-480nm), the surfactant in solution is primarily in the *trans* state (more hydrophobic state and favorable for DNA binding), whereas UV-light (365 nm) illumination converts the surfactant to a larger hydrophilic molecule with a larger dipole moment.

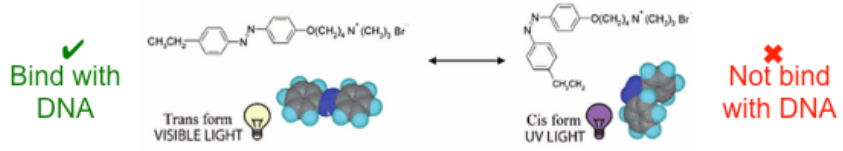

Figure 2-2 Photoisomerization and DNA affinity of AzoTAB.

Azobenzene surfactant incorporated systems can be used as photoswitches, inducing rapid and reversible control over a wide variety of chemical, mechanical, electronic, and optical properties. André Estévez-Torres *et al.* [27] applied azoTAB in DNA compaction and they proposed that the

compaction/decompaction with azoTAB can be used to control gene activity *in vitro*. Figure 2-3 shows the photoisomerization of azoTAB and DNA compaction [27].

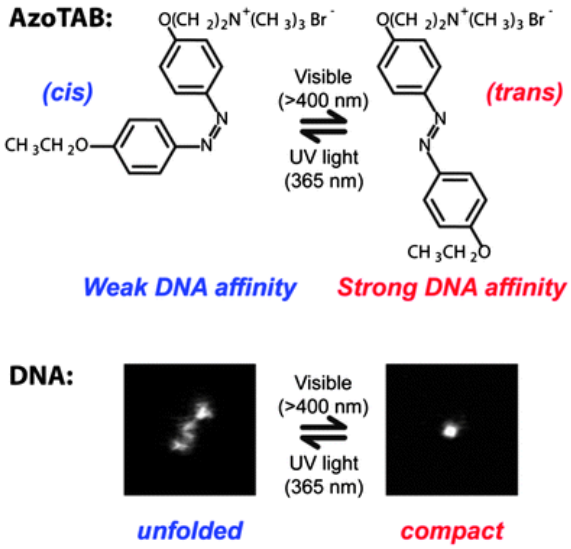

Figure 2-3 Photoisomerization of AzoTAB and DNA compation

2.1.3 DNA assisted Light-induced Self-assembly (LISA) Motivation

Tunable self-assembly induced by light is of continuing interest as a promising approach to new structures and materials with potential applications in optics, sensing, and drug delivery [1] [2] [28]. Rafal Klajn *et al.* reported a reversible crystalline assembly of 4,4-bis(11-mercaptoundecanoxy) azobenzene (ADT) capped gold nanoparticles [29].

DNA assisted self-assembly is programmable and tunable due to the specific recognition between complementary single-stranded DNA. Once we combine this programmability by DNA and the controllability by light, we can create more complex and flexible structures and materials that have wide applications. However, there is not yet any literature showing a systematic study on DNA assisted LISA with azoTAB surfactants. In my study, I started from scratch and worked on the properties and mechanisms of DNA assisted LISA with gold nanoparticles.

2.1.4 Light Induced Self-assembly and Reversibility

Due to the reversibility of azoTAB photoisomerization, the aggregation and dispersion of nanoparticles should be reversible. In order to probe deeper into the reversibility of the system, all the samples were illuminated under alternate UV and blue light. The hydrodynamic diameter was measured by dynamic light scattering (DLS). It is noticeable that DLS also shoot light onto the sample, but the impact on the sample is negligible due to the low intensity and wavelength range of the light.

2.2 Experimental Section

2.2.1 Materials

2.2.1.1 Initial States of AzoTAB Surfactant in solution

Thermodynamically, the *trans* and *cis* isomers of azoTAB can coexist in the phosphate buffer (10mM PB) solution. Before each experiment with azoTAB, the initial state needs to be confirmed. Simply, the color of *trans* and *cis* states of azoTAB in solution is different visually. Figure show a picture of two different states. AzoTAB solution was exposed under blue light (λ=470nm) for one hour to ensure a *trans* initial state before mixing with DNA capped gold nanoparticles.

2.2.1.2 Preparation of DNA Capped Gold Nanoparticles

5nm, 10nm, and 15nm gold nanoparticles (AuNPs) were purchased from TED PELLA, Inc. The nanoparticles are citrate stabilized with a net negative surface charge and dispersed in water. DNA oligonucleotides were purchased from IDT. DNA oligonucleotides were purified by Illustra MicroSpin G-25 Columns and then mixed with AuNPs. The mixture of DNA and AuNPs then went under a NaCl salt aging to a final concentration of 0.1M. After salt aging, the mixture was kept overnight and then centrifuged to remove excessive DNA for 3-4 times.

AuNPs were used as the hard core in this part of experiment. The actual size of the AuNPs was confirmed to be 13nm by DLS. 30-base single-strand DNA (ssDNA) molecules were capped onto AuNPs. Then the capped particles were washed in 0.3M NaCl solution. As was mentioned in the abstract, azoTAB is going under *trans-cis* isomerization under UV illumination and is reversible under blue light. AzoTAB powder was mixed in 0.1M NaCl solvent to a final concentration of 10mM. Then the solution was illuminated under blue light for 1 hour to ensure the initial state of azoTAB molecules are dominantly *trans* azoTAB. Figure 2a shows the DLS size distribution of AuNPs after adding azoTAB, UV light (365nm) illumination, and blue light (470nm) illumination. The photoisomerization of azoTAB is instant and reversible in solution. When alternate UV and blue illumination was introduced, reversible dispersion and aggregation were observed. Figure 2b shows the size change of the reversible dispersion and aggregation. The size of the ssDNA capped AuNPs is 23nm. When azoTAB is added, the major size goes up to 350nm and shows a wider distribution, indicating different sizes of aggregation in the solution. After UV light illumination, the major size goes back down to 22nm, indicating the disappearance of the previous aggregation. After blue light illumination, the major size goes up to 360nm and a wider distribution again.

2.2.2 Instruments and Devices

The 365nm UV light we used is a hand-held 6-watt lamp purchased from VMR products. The 470nm blue light is from a LED spotlight purchased from Edmund Optics.

Dynamic light scattering (DLS) was applied to measure the hydrodynamic diameter of the aggregation and dispersion. Small angle X-ray scattering was applied to probe the interparticle distance. Small angle X-ray scattering (SAXS) experiments were done at National Synchrotron Light Source, beam line X-9A, located inside Brookhaven National Laboratory.

2.3 Results and Discussions

2.3.1 Light Switchable Aggregation and Dispersion

5nm gold nanoparticle (hydrodynamic diameter 7.8nm under DLS) was functionalized with 60-base DNA oligonucleotides. The particles are well dispersed in the solution before the injection of azoTAB solution. The hydrodynamic diameter of the DNA functionalized AuNPs is 17nm in 0.3M PBS buffer (0.3M NaCl in 10mM phosphate buffer). After the injection of azoTAB solution (10mM azoTAB in 0.3M PBS), the hydrodynamic diameter increased dramatically to 360nm in 10 seconds, indicating a rapid aggregation of AuNPs. The ratio of DNA base and azoTAB molecule is approximately 1:1 in the solution. DLS measurement is not accurate when the sample has precipitation (usually when size reaches micro scale). Therefore, the sample was taken out of DLS at 600nm and immediately exposed to 365nm UV light. The hydrodynamic diameter dropped back to approximately 21 nm after 20 minutes, indicating a re-dispersion of AuNPs in solution. Then the sample was taken to 470 nm blue light for 20 minutes. The diameter went up to 360nm. When we continued to switch the illumination from UV to blue, we found the aggregation and dispersion of AuNPs also continued. Then we started to alternate UV and blue illumination for 7 times. A controllable and reversible aggregation was found. shows the DLS measurement of the hydrodynamic diameter. From (a) we can see the AuNPs aggregation and dispersion due to AzoTAB and from (b) we can see the reversibility of the system.

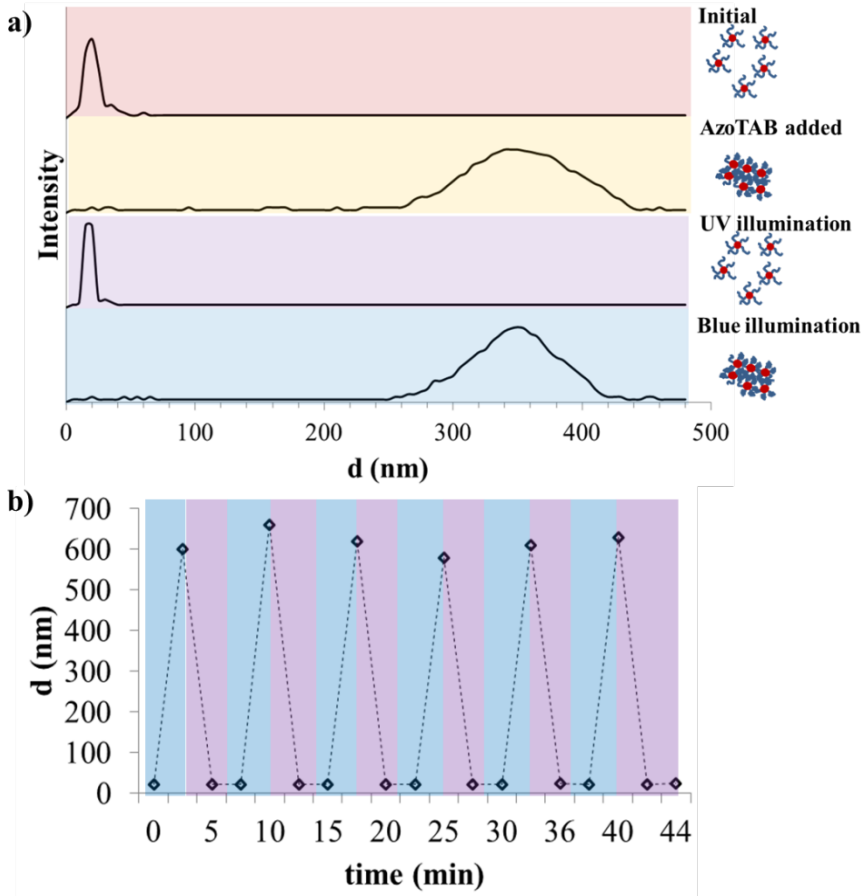

Figure 2-4 a) DLS measurement of AuNP dispersion and aggregation; b) Reversibility under alternate UV/blue illumination

In order to explain the aggregation and dispersion of nanoparticles, we need to understand how the aggregation forms and deforms in the salt solution. DNA molecule is negatively charged due to its phosphate group backbone. The negative charges bring repulsion forces between DNA molecules and therefore keep them from condensation. The negative charged DNA shell also prevents nanoparticles from aggregation. However, the repulsion inhibits more DNA molecules from being grafted onto nanoparticles. That is the reason why salt aging is introduced. The cations in the salt solution can neutralize the negative charges locally, so that more DNA molecules can be attached to nanoparticles. Finding the equilibrium between negative charges and cations is important to make sure enough DNA molecules are attached and the repulsion is strong enough to prevent condensation. If too many negative

charges are neutralized, the repulsion will not be strong enough to keep the DNA shell "stretched". Without the negatively charged DNA shell, nanoparticles will aggregate to minimize surface energy. The *trans* azoTAB molecules have strong DNA affinity and can cause DNA condensation. When the DNA shell collapses, aggregation forms. On the other hand, *cis* azoTAB molecules are not favorable for DNA binding, so the DNA molecules will unfold and the negatively charged DNA shell will bring the particles back to dispersion.

2.3.2 Comparing Self-assembly in Sodium (NaCl) and Magnesium cation ($MgCl_2$) Environment

Gold AuNPs were used as the hard core in this part of experiment. The actual size of the AuNPs was confirmed to be 13nm by DLS. 30-base single-strand DNA (ssDNA) molecules were capped onto AuNPs. Then the capped particles were washed in 0.1M NaCl solution. AzoTAB powder was mixed in 0.1M NaCl solvent to a final concentration of 10mM. Then the solution was illuminated under blue light for 1 hour to ensure the initial state of azoTAB molecules are dominantly *trans* azoTAB. AzoTAB was mixed with AuNPs to a molecular ratio of 400 azoTAB molecule per DNA base. DLS was used to measure the size change of the AuNPs. Figure 2-5 shows the aggregation and dispersion of AuNPs after azoTAB is introduced. Fast aggregation formed once the azoTAB was mixed with AuNPs in the solution. When UV illumination was introduced, the aggregation quickly disappeared. When blue illumination was introduced, aggregation formed again. The aggregation-dispersion process was proved to be reversible.

From our previous study, we found that magnesium cations are very strong competitors against azoTAB molecules towards DNA binding. With the presence of magnesium cations, azoTAB induced aggregation is severely hindered. Gold AuNPs were used as the hard core in this part of experiment. The actual size of the AuNPs was confirmed to be 14nm by DLS. 30-base poly-T single-strand DNA (ssDNA) molecules were capped onto AuNPs and the particles were dispersed in 4mM $MgCl_2$. AzoTAB powder was mixed in 4mM $MgCl_2$ solvent to a final concentration of 10mM. Then the solution was illuminated under blue

light for 1 hour to ensure the initial state of azoTAB molecules are dominantly *trans* azoTAB. The ratio of azoTAB:DNA was set at 800:1. This ratio is much higher than that in sodium environment.

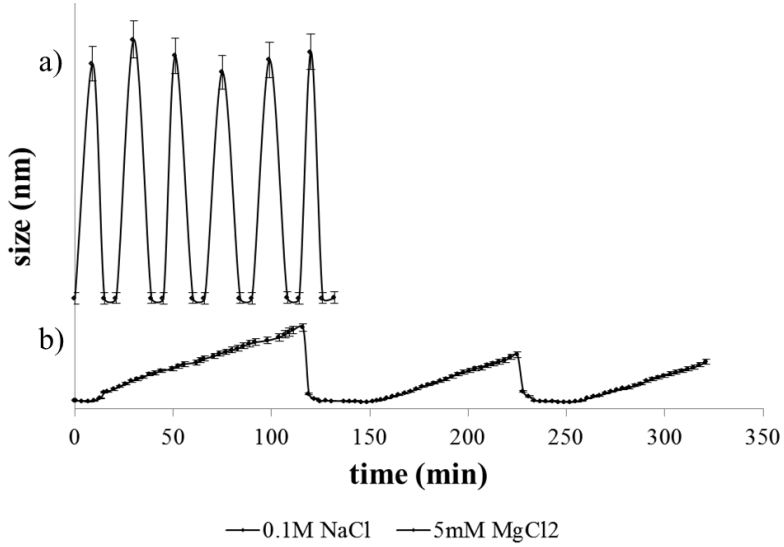

Figure 2-5 Reversibility of 15nm AuNP capped with 30-polyT DNA in a) 0.1M NaCl and b) 5mM MgCl2 environment

Figure 2-5 shows the aggregation and dispersion of AuNPs. In Figure 3a, in NaCl environment when azoTAB is introduced, the aggregation size quickly reaches to 600nm. Under UV light illumination, the size drops quickly back to 25nm. Under blue light illumination, the size goes up quickly to 600nm again. Each high-low cycle takes approximately 15-18 minutes. Compared to the aggregation and dispersion in NaCl solution, even though the azoTAB ratio is higher, the aggregation was still slowly and the aggregation size is smaller. However, when the UV was introduced, the aggregation disappeared quickly just as the situation in NaCl solution. Under blue illumination, the size goes up slowly to 200nm. The slow aggregation was caused by the competition between *trans* azoTAB and Mg^{2+} cations to bind with DNA bases. The ionic strength of 0.1M NaCl is 0.1 and 0.15 for 5mM $MgCl_2$. When UV was introduced, *trans* azoTAB becomes *cis* azoTAB and do not bind with azoTAB. There is no more competition with the cations in the solution.

2.3.3 DNA Condensation

From our studies, we found that before visible aggregation under DLS measurements, sometimes we can observe particle size shrinking. Because our sample has gold hard core and soft DNA shell, it would be

safe to say that the DNA shell is condensed from its stretchy state to a compacted state. DNA condensation is more visible under DLS at low azoTAB concentrations. This is mainly due to the presence of excessive azoTAB can bind DNA molecules and induce aggregation faster.

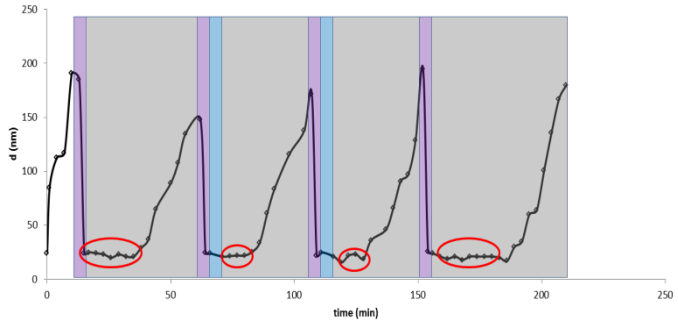

Figure 2-6 DNA condensation of 15nm AuNPs in 0.02M NaCl

Figure 2-6 shows the visible DNA condensation of 15nm AuNPs in 0.02M NaCl solution with low azoTAB ratio. From this figure, we can observe DNA condensation before each aggregation formed. We proposed a mechanism to explain how azoTAB induces aggregation. We believe that DNA condensation can cause a loss of surface charges offered by DNA molecules. Without enough charges, the repulsion is not strong enough to keep AuNPs from aggregate to lower surface energy.

Figure 2-7 shows DNA condensation and compares the sizes with DNA capped particles (24nm under DLS measurement) and particles without DNA shell (14nm under DLS measurement). The size of the sample is in between. After blue illumination, the size goes down to nearly the same as the "naked" free AuNP (AuNP without DNA shell), which indicates that the DNA shell is highly condensed. This phenomenon is confirmed using SAXS as interparticle distance is quenched with the presence of *trans* azoTAB (see Section 2.3.5). Then the size starts to go up, indicating the initiation of particle aggregation in the solution.

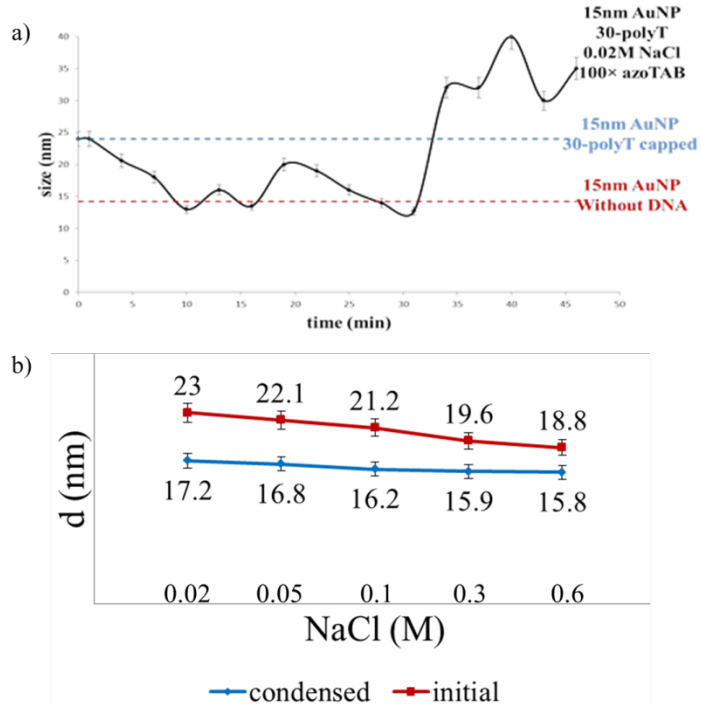

Figure 2-7 a) DLS measurement of DNA shell condensation with azoTAB
b) DNA shell condensation in NaCl solution as a control group

2.3.4 Controllable Parameters

2.3.4.1 Core Particle Size

In this part of experiment, three different sizes of AuNP hard core were tested. The sizes are 7nm, 11nm, and 15nm under DLS measurement. 30-base poly-T single-strand DNA (ssDNA) molecules were capped onto AuNPs and the particles were dispersed in 0.1M NaCl. The concentration of AuNPs was controlled at 50nM. Figure 2-8 shows the aggregation and dispersion of AuNPs. In Figure 2-8a, aggregation size goes up to 750nm and each high-low cycle takes approximately 15 minutes. In Figure 2-8b, the aggregation size reaches to 600nm and a high-low cycle takes about 20 minutes. In Figure 2-8c, the aggregation size goes up to only 175nm and each high-low cycle is as slow as 35 minutes. From the curves, we can easily tell that the larger the AuNPs are, the faster the aggregation and dispersion is. By comparing the reversibility of the three sizes, we found the 15nm AuNPs have the best reversibility.

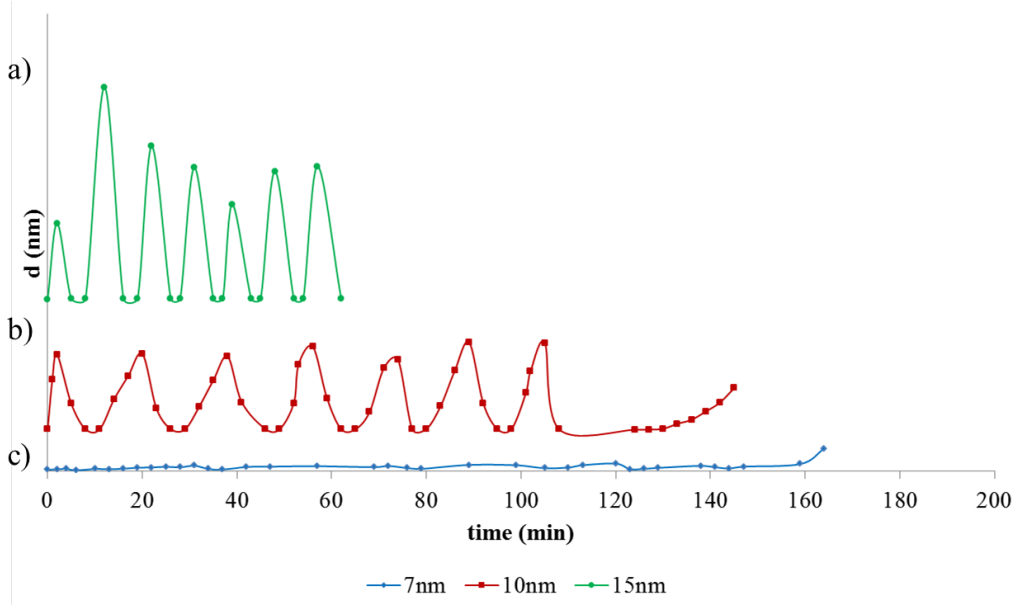

Figure 2-8 The aggregation and dispersion of a) 15nm AuNPs b) 10nm AuNPs c) 7nm AuNPs in 0.1M NaCl

2.3.4.2 Ratio of AzoTAB molecules per DNA base

In our experiments, we tested more than five different ratios of azoTAB. We can conclude that higher azoTAB ratio leads to faster aggregations. However, there is no difference in UV illumination. Here we propose a diffusion limited reaction assumption to explain the observation.

To look more into the light induced aggregation-dispersion process. We designed different illumination strategies. After first UV illumination for 4 minutes, sample was kept in DLS chamber and DLS was programmed to measure every 3 minutes. This was considered as a control group to show the degree of DLS laser would affect the aggregation process. After the second UV illumination for 4 minutes, sample was continuously illuminated under blue light for 5 minutes. After the third UV illumination for 4 minutes, the sample was continuously illuminated under blue light for 3 minutes. After fourth UV illumination for 4 minutes, sample was continuously illuminated under blue light for 1 minute and then kept in DLS chamber for measurements. After fifth UV illumination for 4 minutes, sample was continuously illuminated under blue light for 30 seconds then kept in DLS chamber for measurements. After sixth UV illumination for 4 minutes, sample was kept in DLS chamber again (same as after the first UV illumination).

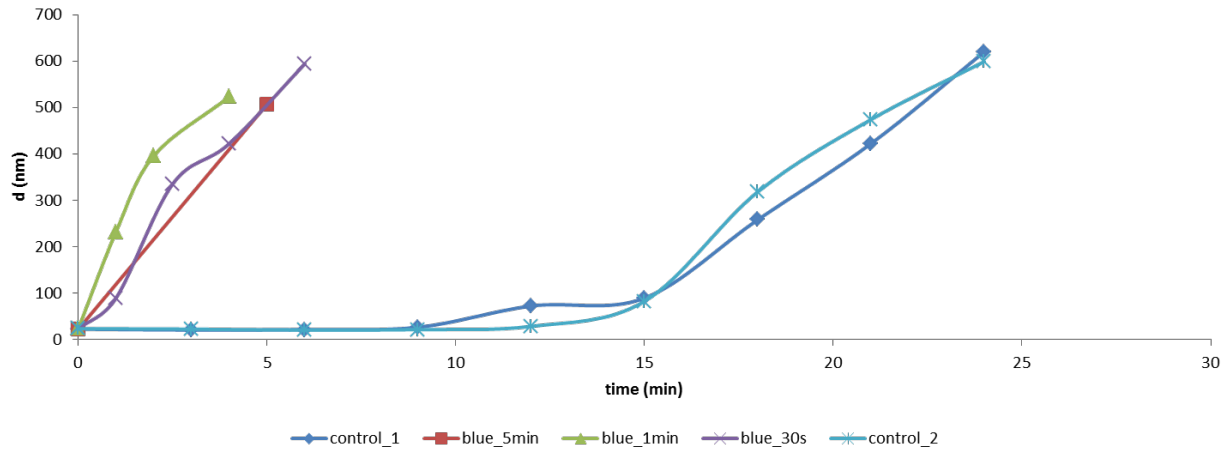

Figure 2-9 Different illumination strategies for 15nm AuNPs in 0.02M NaCl solution with azoTAB:DNA ratio of 400:1.

Figure 2-9 shows the aggregation after each UV illumination. Control 1 and control 2 show that aggregation was more slowly without blue illumination. Even with blue illumination as short as 30 seconds, aggregation can be induced as shown in the figure. However, it is noticeable that the length of illumination time doesn't change the aggregation rate drastically. Here we propose the mechanism as "diffusion limited". From our previous studies, we found that the process of azoTAB photo isomerization is instant. That means, only very short illumination is actually needed to switch azoTAB between *cis* and *trans* states. The reason why aggregation and dispersion of particles take much longer time is that particles need to diffuse in the solution, in order to form aggregation or disperse.

2.3.4.3 Salt Concentration

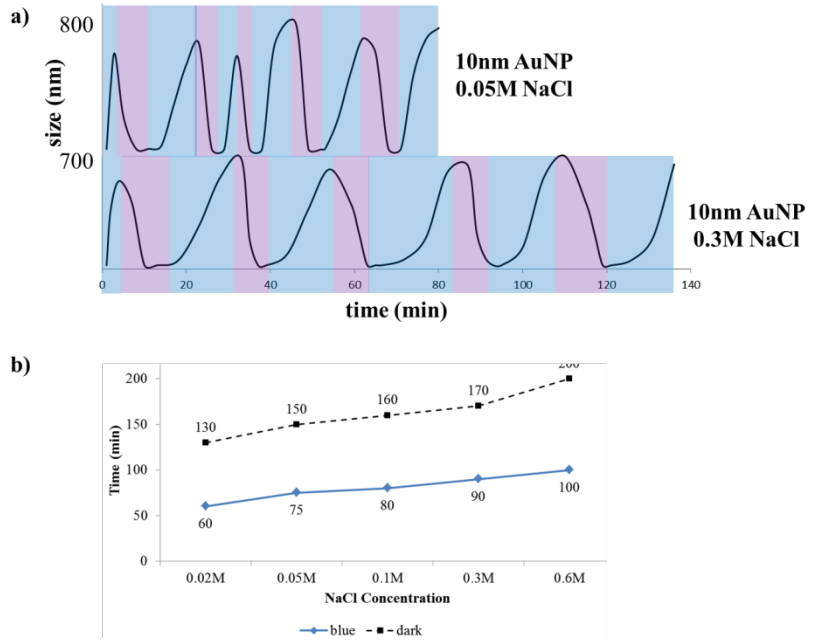

Figure 2-10 a) Reversibility in different NaCl concentrations; b) Aggregation time in different NaCl concentrations

Figure 2-10 shows the reversibility of 10nm AuNP in low salt concentration (0.05M NaCl as an example) and high salt concentration (0.3M NaCl as an example). In both concentrations, the reversibility of AuNP is observed. In low salt concentration, it takes approximately 17min to complete a cycle. The aggregation size is observed as 800nm. In high salt concentration, it takes approximately 23 min to complete a cycle. The aggregation size is observed as 700nm. Figure 2-10b shows the aggregation time in different salt concentrations. The higher the salt concentration is, the longer it takes to aggregate and the smaller the aggregation size can reach.

As mentioned, the mechanism of interaction between azoTAB and DNA is not yet clarified. Here I present three assumptions to explain the interaction. First, azoTAB molecule has a positive charge. This positive charge makes azoTAB attracted to DNA and therefore a competitor against cations in the solution. This type of binding is non-specific and primarily electrostatic. Second, *trans* azoTAB can bind in the grooves of DNA, which is a type of binding combines electrostatic and hydrophobic interaction.

Lastly, π-π bonding can form between the DNA base and the phenyl group in azoTAB molecule. This type of binding requires a planar or approximately planar structure, which only exists in *trans* azoTAB.

2.3.5 Small Angle X-Ray (SAXS) Results

In SAXS experiments, first measurement was taken after the azoTAB injection. Using free AuNPs as background, one peak shows in the S(q)-q curve, indicating an aggregation and the interparticle distance (center to center distance) to be 22nm (see Figure 2-11). The hard core (without the DNA shell) of the functionalized particle is 6-8nm, which indicates a surface-to-surface distance of less than 1nm. This small distance reveals that the DNA shell over the AuNP is collapsed due to the condensation of DNA shell over the particle. This condensation of DNA was also observed by DLS measurement that will be illustrated in previous chapters. After the sample was exposed under 365nm UV light for 20 minutes, the peak in S(q)-q curve disappeared (Figure 2-11b), indicating the particles were dispersed like free particles in the solution. The sample was then put into a dark box overnight. The peak in S(q)-q curve appeared again at an interparticle distance of 22nm (Figure 2-11c), indicating the aggregation of the particles. This experiment reveals that the *cis* to *trans* conversion of azoTAB occurs without blue light illumination.

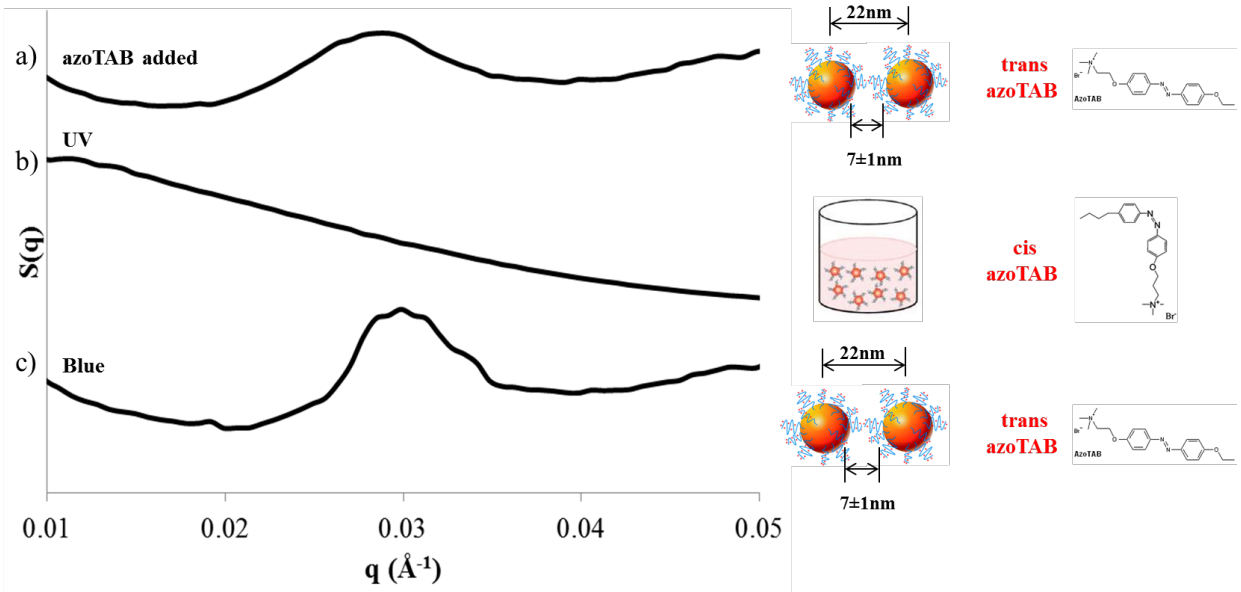

Figure 2-11 SAXS measurement of (a) after azoTAB injection; (b) after UV illumination; (c) after blue illumination

Consistant SAXS results for 11±1 nm particles (capped with 30 poly-T single strand DNA) were collected (see Figure 2-12). Firstly, the particles were measured as background. Then azoTAB was added into the sample. After UV illumination and blue illumination, the sample was measured respectively. When the background was subtracted from the data, we found there was no peak after UV illumination and there is a single peak after blue illumination. The q value of the single peak is 0.02845Å^{-1}, which yielded the interparticle distance (core to core) to be around 22nm and the distance between particles (edge to edge) to be 7±1nm.

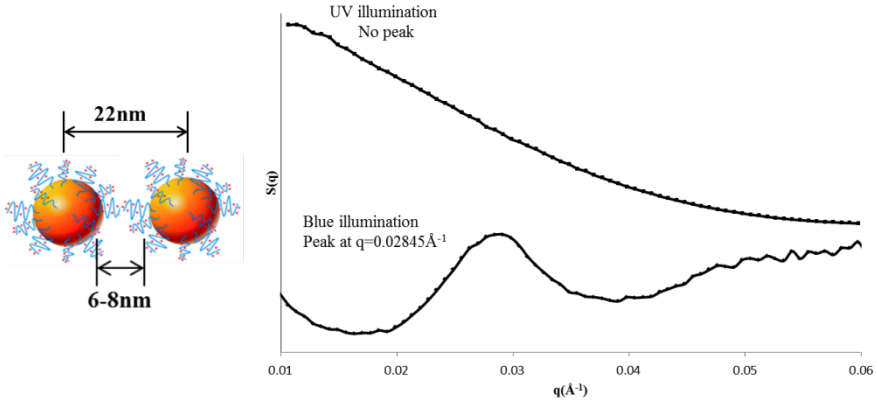

Figure 2-12 SAXS Results for 15nm AuNPs system

2.3.6 State Diagram

Figure 2-13 shows the state diagram of the interaction between 15nm AuNP and azoTAB in various concentrations. The diagram can help us find the right combination of concentrations for different experiments.

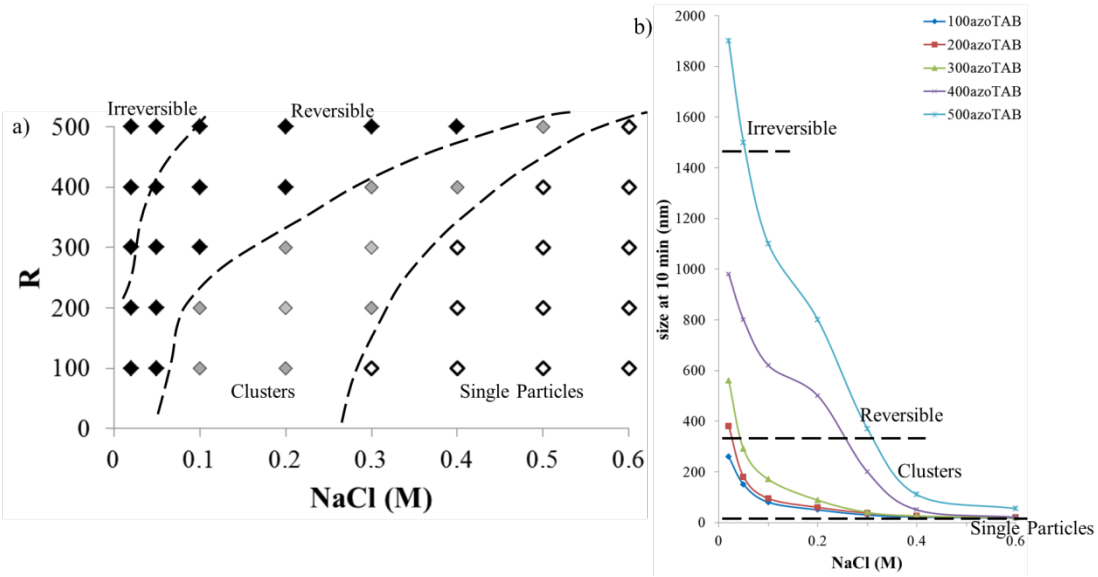

Figure 2-13 a) State diagram of R (azoTAB ratio) versus NaCl concentration b) Aggregation sizes at 10 minute when R (azoTAB ratio) is controlled.

To understand the state diagram, we first look at it horizontally, which means we control azoTAB ratio and vary the NaCl concentration. In this case, the higher the concentration is, the slow and small the aggregation is. When the NaCl concentration is within low regime (0-0.05M), the aggregation observed is very fast. The size of the aggregation can reach 2000-3000nm instantly. This fast aggregation makes it very difficult for UV illumination to penetrate. Thus, this kind of aggregation is considered to be "irreversible". When the NaCl concentration is within mediate regime (0.05-0.3M), the aggregation forms in a reasonable and controllable speed. This regime is considered to be the best experimental regime. When the NaCl concentration reaches high regime (0.3-0.6M), aggregation forms very slowly. In this case, DNA condensation is observed. The DNA molecules on the surface of the AuNPs are compacted. The size of the capped particle is closed to a naked particle. Figure 9b shows the aggregation sizes at 10

minute (the moment when injecting azoTAB is considered 0 in different salt concentrations when the azoTAB ratio is controlled. Then we look at the state diagram vertically. That is, we control the NaCl concentration and vary the ratio of azoTAB. In this case, the higher the concentration is, the slow and small the aggregation is. When the azoTAB ratio is within high regime (500-600), the aggregation observed is very fast. The size of the aggregation can reach 2000-3000nm instantly. This fast aggregation makes it very difficult for UV illumination to penetrate. Thus, this kind of aggregation is considered to be "irreversible". When the azoTAB ratio is within mediate regime (300-500), the aggregation forms in a reasonable and controllable speed. This regime is considered to be the best experimental regime. When the azoTAB ratio falls within low regime (100-200), aggregation forms very slowly. In this case, DNA condensation is observed. The DNA molecules on the surface of the AuNPs are compacted.

2.3.7 Interplay with Double-Strand DNA and DNA Hybridization

Magnesium cations are favorable for DNA hybridization and the effect of azoTAB on DNA hybridization is not clear. To probe the interplay with DNA hybridization, complementary DNA strands were introduced into the system. AuNPs were divided into two groups A and B. Group A was functionalized with 30-base DNA single strands A, while group B was functionalized with 30-base complementary DNA strand B. The length of complimentary part is 15 bases. Figure 2-14 shows an illustration of the system.

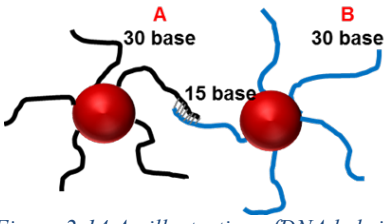

Figure 2-14 An illustration ofDNA hybridization on AuNPs

From our study, we found that magnesium cations are very strong competitors against azoTAB molecules towards DNA binding. With the presence of magnesium cations, azoTAB induced aggregation is severely hindered. This time, 15nm AuNPs were capped with 30-base poly-T DNA and dispersed in 5mM $MgCl_2$. The ratio of azoTAB:DNA was set at 800:1. This ratio is much higher than that in sodium environment.

Figure 2-15 shows the aggregation caused a) only by DNA hybridization, b) only by azoTAB, and c) by DNA hybridization and azoTAB.

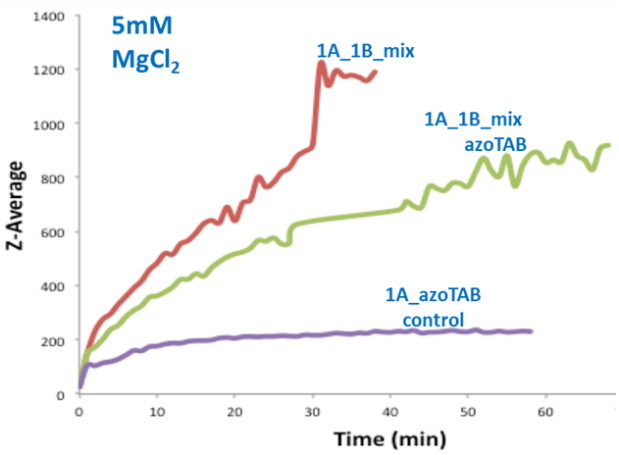

Figure 2-15 Aggregation caused by azoTAB and DNA hybridization in 5mM $MgCl_2$.

Compared to magnesium cations, sodium cation is not as competitive with azoTAB in the solution. Thus, the aggregation is more dominantly controlled by azoTAB. Figure 2-16 shows the difference between azoTAB and DNA hybridization caused aggregation. When the azoTAB ratio is higher (400 azoTAB per DNA base), aggregation caused by only azoTAB and by combination of azoTAB and DNA hybridization is nearly the same. In this case, the aggregation is dominantly caused by azoTAB binding with DNA. The aggregation speed is faster than that caused by only DNA hybridization. When the azoTAB ration is lower (100 azoTAB per DNA base), the hybridization is slightly hindered by azoTAB. When UV illumination is introduced, the aggregation caused by azoTAB disappears.

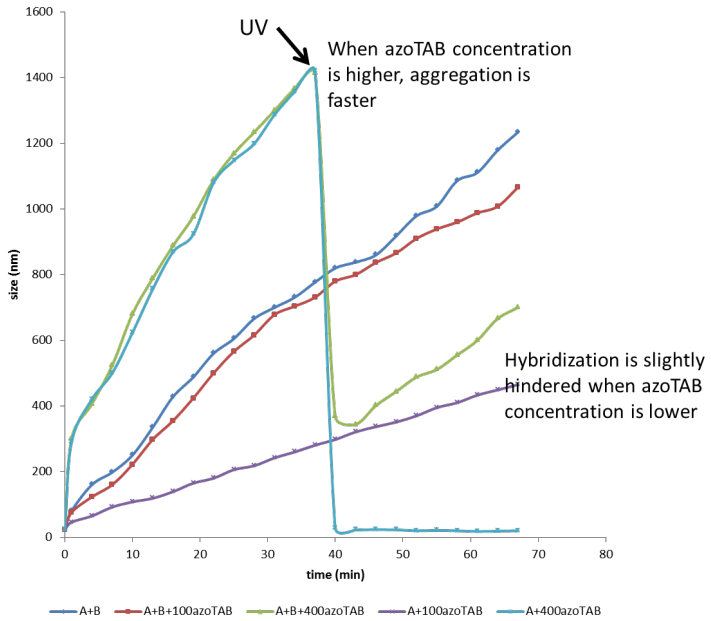

Figure 2-16 DNA hybridization in low and high azoTAB ratios in 0.1M NaCl.

2.3.8 UV induced self-assembly

In Section 2.3.6, we summarized the interaction between azoTAB and DNA capped AuNPs in a phase diagram. From the phase diagram, we can find a regime where the DNA shells on the particles are condensed due to azoTAB but no assembly is induced. When DNA strands are condensed, it is not likely to hybridize normally. In this case, AuNPs capped with complementary DNA strands can co-exist in solution without inducing any self-assembly. If we introduce UV illumination at this moment, DNA strands will stretch back to "worm-chain" state and ready to hybridize. Thus, UV induced self-assembly happens. Compare to our previous experiment, the assembly is induced by UV light instead of by blue light. The assembly is programmable and controllable thanks to the merits of DNA hybridization. Figure 2-17 shows the strategy of UV induced self-assembly experiment.

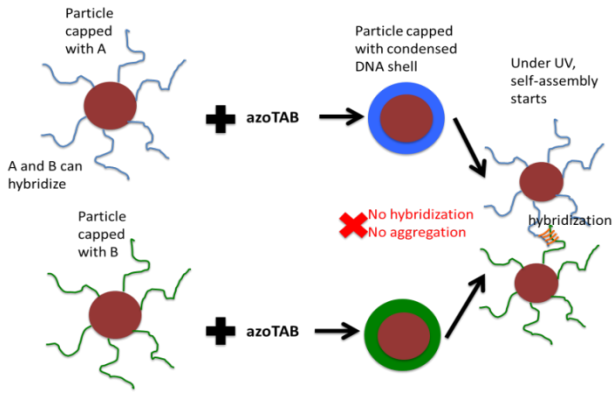

Figure 2-17 The strategy of UV induced self-assembly experiment.

Figure 2-18 shows the DLS measurement of UV induced self-assembly. In this experiment, two types of DNA strands are capped onto 15nm AuNPs. The two types of DNA are complimentary. The AuNPs capped with the two types of DNA are named as A and B respectively. 30nM A and B are separated in two tubes. Each tube is mixed with azoTAB at azoTAB:DNA ratio of 400:1. DLS measurements showed that the DNA shells were condensed. Then A and B were mixed together and put under DLS measurements. From the measurements, we can see the hybridization was severely hindered. When the UV illumination was started, we observed a slight drop of size under DLS. This slight drop was caused by disassembly of azoTAB induced aggregation. After the slight drop, an aggregation was observed. This aggregation was due to DNA hybridization. AuNPs capped with same DNA were tested as a control group.

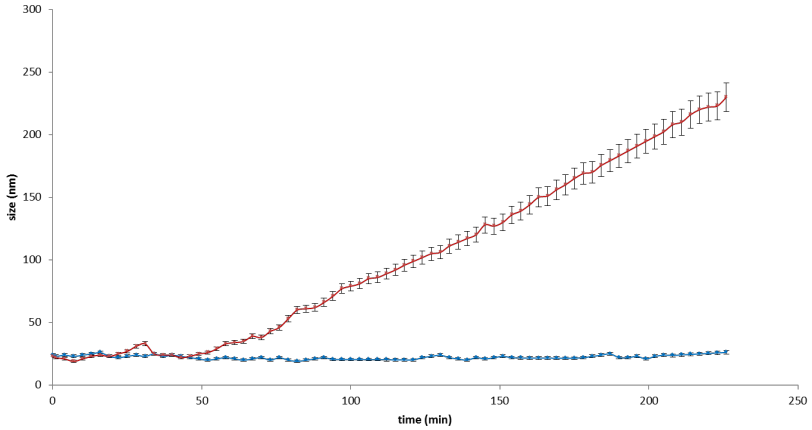

Figure 2-18 DLS measurement of UV induced self-assembly

2.4 Conclusions

AzoTAB surfactants have *trans* and *cis* photoisomerization in solution. Under blue illumination, *trans* azoTAB dominates, which has strong DNA affinity and can cause DNA condensation. Once the DNA molecules condensate, the negatively charged DNA shell over nanoparticles collapses and nanoparticles will start to aggregate to minimize surface energy. Under UV illumination, *cis* state dominates, which is not favorable for DNA binding and DNA molecules can unfold and the negative charges will bring the nanoparticle apart. DLS and SAXS measurements showed evidences for the aggregations and dispersions of AuNPs.

Three assumptions were proposed in this studies attempting to explain the interaction between DNA molecules and azoTAB surfactants: (i) azoTAB molecule has a positive charge, this positive charge makes azoTAB attracted to DNA and therefore a competitor against cations in the solution. This type of binding is non-specific and primarily electrostatic; (ii) *trans* azoTAB can bind in the grooves of DNA, which is a type of binding combines electrostatic and hydrophobic interaction; (iii) π-π bonding can form between the DNA base and the phenyl group in azoTAB molecule. This type of binding requires a planar or approximately planar structure, which only exists in *trans* azoTAB.

As a good support to the assumptions, the concentration of cations in the solution has a noticeable effect on the interaction between azoTAB and DNA molecules. When the concentration increases, more positively charged cations compete with azoTAB and decrease the binding chances between azoTAB and DNA molecules.

Three major controllable parameters were studied. For core particle size, the bigger it is, the larger and faster the aggregation is. Therefore, the worse the reversibility is. For azoTAB/DNA ratio, the bigger the ratio is, the larger and faster the aggregation is. Thus, the worse the reversibility is. For the salt concentration, the bigger it is, the smaller and slower the aggregation is. To present these parameters, a

state diagram was made. The state diagram also lead us to find a condition where the self-assembly can be induced by UV (compared to the blue light induced self-assembly).

Magnesium cations favor DNA hybridization. The presence of azoTAB will inhibit DNA hybridization. This inhibition may come from the π-π bonding between DNA base and planar azoTAB phenyl group.

3 Diffusion of Nanoclusters

3.1 Introductions

3.1.1 Nanoclusters

The self-assembly of finite-sized nanoclusters is considered to mimic the formation of molecules and offers valuable information. With the development of DNA origami technology, more complex and novel structures can be designed and fabricated. In this study, two different nanoclusters were fabricated in our group: (i) a 3-dimensional octahedron structure. Six-bundled DNA origami structure form the frame of the octahedron and six 10nm AuNPs seat at the corners. (ii) a 2-dimensional flat tile with a 10nm AuNP centered in the middle. Figure shows the structure of the nanoclusters.

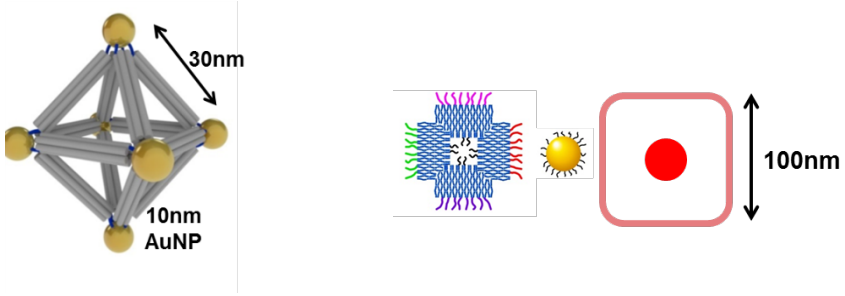

Figure 3-1 An illustration of the nanostructures: octahedron and 2D tile.

3.1.2 Instrument: Nanosight LM-10HS

Nanosight LM-10HS is composed of four basic parts: (i) a conventional optical microscope to observe particle movement; (ii) a laser light source to induce scattering from the particles; (iii) a video recorder connected to the microscope; (iv) a sample chamber approximately 40 μL in volume. The resolution of the instrument equals to half the wavelength of the laser light source. In this study, a green laser ($\lambda \approx 500$nm) was chosen and the resolution is approximately 250nm by

250nm, which is not able to visually distinguish nanoclusters from single particles. This resolution limit requires a homogenous sample. When the laser was shot onto the particles in the solution, light is scattered and many bright dots are recorded through the microscope. By tracking the projection of each dot between frames (0.033s) and analyzing the trajectories, diffusion properties are probed from the mean square displacement curve (MSD~τ curve) and the displacement probability histogram. Figure 3.2 shows the picture of the instrument and some examples of the analysis.

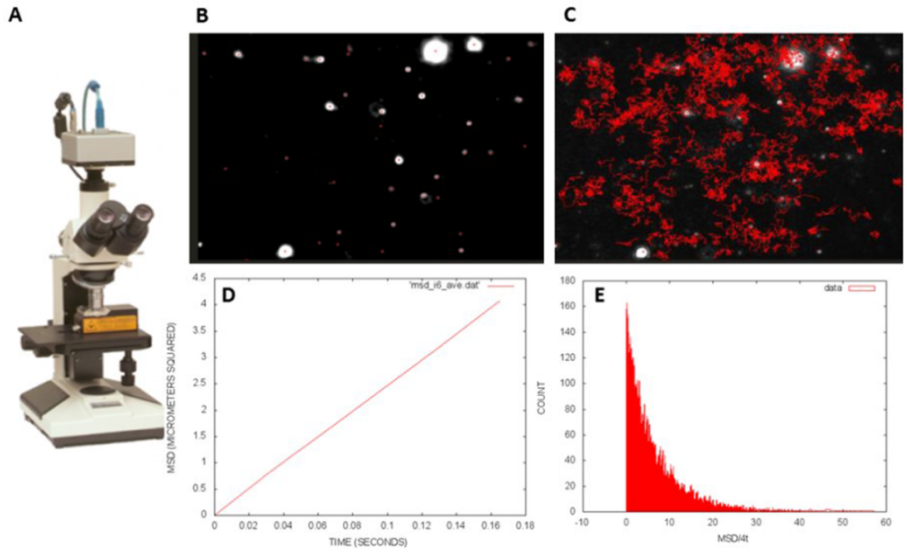

Figure 3-2 The setup of Nanosight LM-10HS

As mentioned in Section 1.3, for 2-dimensional diffusion, the mean square displacement (MSD or $<x^2>$ is related to the diffusion coefficient D as follows:

$$< x^2 >= 4D\tau$$

The slope of the MSD~τ curve $\tan\theta = \frac{<x^2>}{\tau} = 4D$ and the diffusion coefficient can be obtained.

3.1.3 Diffusion in Polymer Solutions

A biological medium usually contains a high total concentration of soluble macromolecules. Thus, it is valuable to probe the diffusion in a crowding solution. The presence of polymer can mimic the crowding environment.

In this study, polyethylene glycol (PEG) was used as the polymer solvent for the nanoclusters. The structure of PEG can be simply denoted as H-(O-CH2-CH_2)$_n$-OH. The molecular mass of the PEG in this study is 35,000. The stretched length, or contour length L_0 of this 35k PEG is approximately 275nm.

3.2 Experimental Section

The fabrication of the nanoclusters will not be discussed in this proposal. The protocol used to prepare the nanoclusters cannot provide homogenous sample. In order to obtain homogenous sample, electrophoresis is required. The gel used in the electrophoresis is 1% agarose for both nanoclusters. Atomic force microscope (AFM) and transmission electron microscope (TEM) were applied to check the homogeneousness after electrophoresis.

3.3 Results and Discussions

3.3.1 Octahedron

Figure 3-3 shows the mean square displacement (MSD) curve over time interval in different PEG concentrations. In order to probe the effect of PEG polymer on the diffusion, three different lengths of trajectories were analyzed.

All the trajectories of 100 steps or shorter in length were analyzed. First, in water, with the absence of polymer effect, the octahedron frame moves freely without any entanglement or constraint. The diffusion coefficient is $1.4 m^2 s^{-1}$. Second, in 3% 35k PEG solution, the diffusion of the octahedron slows down and the diffusion coefficient is $0.22 m^2 s^{-1}$. Lastly, in 6% 35k PEG solution, the diffusion coefficient is $0.08 m^2 s^{-1}$. The diffusion coefficient becomes smaller when the PEG concentration becomes higher.

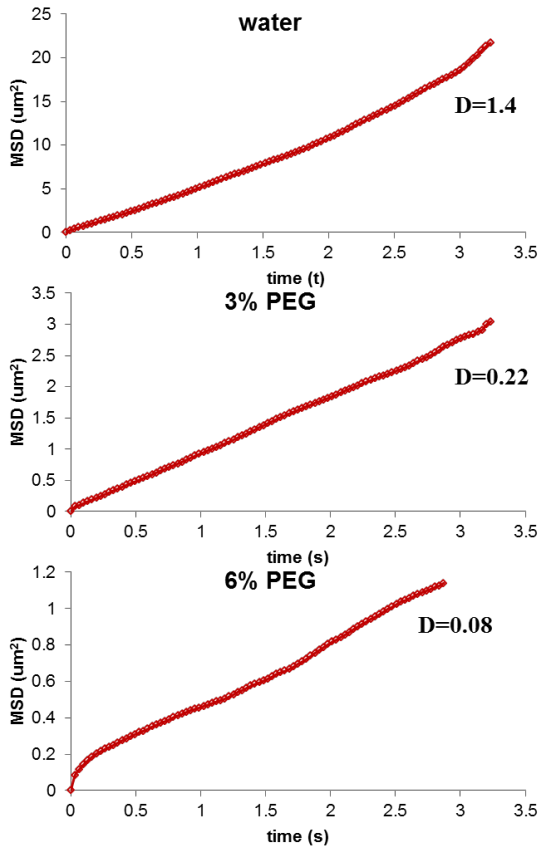

Figure 3-3 MSD curves in different PEG concentrations

It is interesting to think about if the diffusion behavior of octahedron remains the same during traveling To find out the answer of this question, I extracted all the long trajectories from the records and broke them into five parts: (i) the records from step 2 to step 21 (the length is 20 steps); (ii) from step 22 to 41; (iii) from step 42 to 61; (iv) from step 62 to 81; and (v) from step 82 to 101. As a controlled group, the records in water were analyzed in the same way. Figure 3-4 shows the MSD~τ curves of each part, (a) in 6% PEG and (b) in water. From figure a, it is noticeable that the diffusion coefficient of the octahedrons is becoming smaller in their 100-step "journey", which explains the separation in figure c. The entanglement of 6% 35k PEG polymer slows down the octahedron and some polymer remains on the octahedron frame and makes the octahedron appears larger and larger.

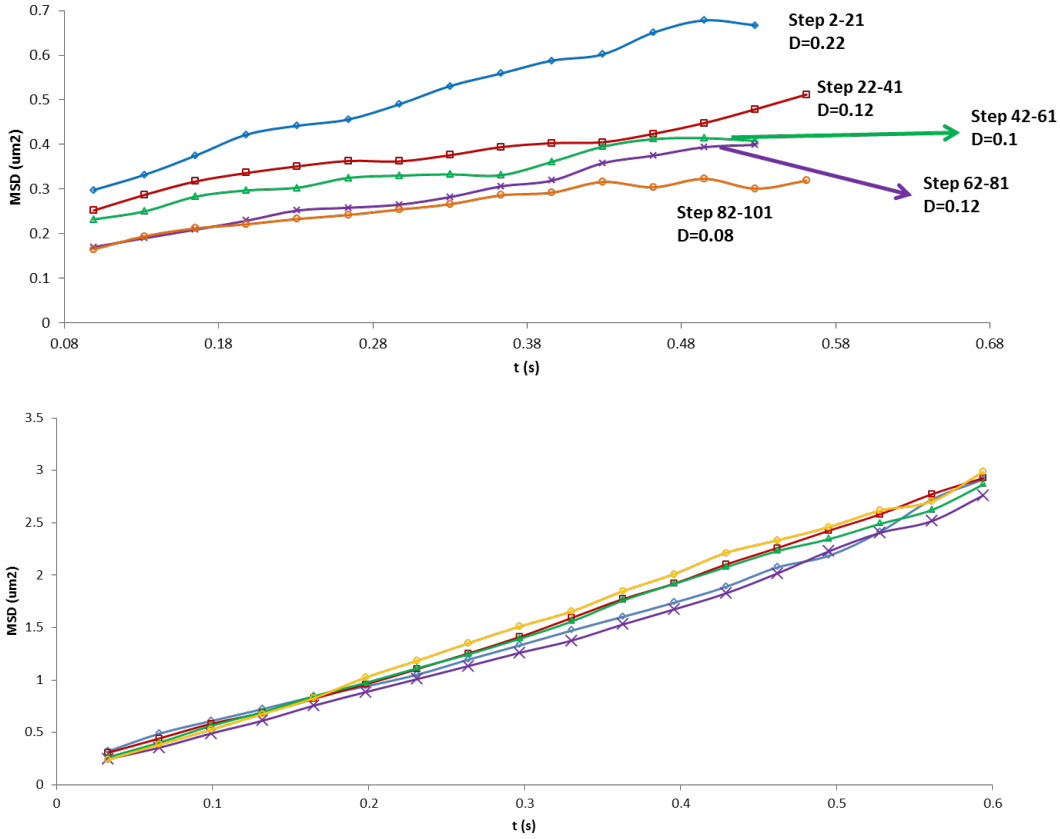

Figure 3-4 Stepwise MSD curve in 6% 35k PEG solution

3.4 Conclusions and Future Work

The presence of polymers brings strong entanglement with nanoclusters. This entanglement is more obvious when the nanocluster is a framed structure like the octahedron in the study. The diffusion coefficient of the octahedron becomes larger during traveling. More works need to be done about this structure.

The frame structure of octahedron brought some interesting results from particle tracking. The diffusion of solid octahedron nanoparticles in polymer needs to be explored. Our group has fabricated solid octahedron gold nanoparticles of similar size. Some control experiments can be designed to probe the diffusion behavior of a simple loop structure. The entanglement between the loop and the polymer is similar to that between the octahedron frame and the PEG, but simpler and easier to study.

4 Bibliography

[1] M. e. a. Grzelczak, "Directed Self-Assembly of Nanoparticles," *Acs Nano,* pp. p. 3591-3605, 2010. 4(7).

[2] O. a. Y. Z. Gang, "Shaping Phases by Phasing Shapes," *Acs Nano,* pp. p. 8459-8465, 2011. 5(11).

[3] N. a. N. K. Seeman, "Optimal-Design of Immobile and Semi-Mobile Nucleic-Acid Junctions," *Biophysical Journal,* pp. p. A93-A93., 1982 . 37(2).

[4] N. Seeman, "DNA in a material world," *Nature,* pp. p. 427-431., 2003. 421(6921).

[5] P. Rothemund, " Folding DNA to create nanoscale shapes and patterns," *Nature,* pp. p. 297-302, 2006. 440(7082).

[6] W. Z. H. W. R. &. S. N. Liu, "Crystalline two-dimensional DNA-origami arrays.," *Angew. Chem. Int. Edn. Engl,* p. 264–267, (2010) 50.

[7] Y. e. a. Ke, "Scaffolded DNA origami of a DNA tetrahedron molecular container," *Nano Lett,* p. 2445–2447, (2009) 9.

[8] E. e. a. Andersen, "Self-assembly of a nanoscale DNA box with a controllable lid. ,," *Nature,* p. 73–76, (2009) 459.

[9] S. e. a. Douglas, "Self-assembly of DNA into nanoscale three-dimensional shapes," *Nature,* p. 414–418, (2009) 459.

[10] H. D. S. &. S. W. Dietz, "Folding DNA into twisted and curved nanoscale shapes," *Science,* p. 725–

730, (2009) 325.

[11] T. H. B. T. J. I. D. &. S. W. Liedl, " Self-assembly of three-dimensional prestressed tensegrity structures from DNA.," *Nat. Nanotechnol.,* p. 520–524, (2010) 5.

[12] B. e. a. Saccà, "Orthogonal protein decoration of DNA origami," *Angew. Chem. Int. Edn. Engl. ,* p. 9378–9383, (2010) 49.

[13] C. e. a. Mirkin, "A DNA-based method for rationally assembling nanoparticles into macroscopic materials," *Nature,* pp. p. 607-609, 1996 382(6592).

[14] A. e. a. Alivisatos, "Organization of 'nanocrystal molecules' using DNA," *Nature,* pp. p. 609-611, 1996. 382(6592).

[15] A. e. a. Stadler, "DNA-incorporating nanomaterials in biotechnological applications," *Nanomedicine,* pp. p. 319-334, 2010. 5(2).

[16] I. e. a. Medintz, "Quantum dot bioconjugates for imaging, labelling and sensing," *Nature Materials,* pp. p. 435-446, 2005. 4(6).

[17] W. M. M. a. U. K. Algar, "The application of quantum dots, gold nanoparticles and molecular switches to optical nucleic-acid diagnostics," *Trac-Trends in Analytical Chemistry,* pp. p. 292-306., 2009. 28(3).

[18] N. a. A. T. Licata, "Statistical mechanics of DNA-mediated colloidal aggregation," *Physical Review E,* 2006. 74(4).

[19] C. a. A. T. Knorowski, "Dynamics of DNA-programmable nanoparticle crystallization: gelation, nucleation and topological defects. , :," *Soft Matter,* pp. p. 12053-12059., 2012. 8(48).

[20] C. F. S. a. F. S. Hsu, "Theoretical Description of a DNA-Linked Nanoparticle Self-Assembly," *Physical Review Letters,* 2010. 105(5).

[21] O. F. L. a. F. S. Padovan-Merhar, "Stability of DNA-linked nanoparticle crystals: Effect of number of strands, core size, and rigidity of strand attachment," *Journal of Chemical Physics,* 2011. 134(24).

[22] S. B. M. a. D. F. Angioletti-Uberti, "Re-entrant melting as a design principle for DNA-coated colloids," *Nature Materials,* pp. p. 518-522., 2012. 11(6).

[23] C. S. B. a. A. T. Knorowski, "Dynamics and Statics of DNA-Programmable Nanoparticle Self-Assembly and Crystallization," *Physical Review Letters,* 2011. 106(21).

[24] B. e. a. Mladek, "Quantitative Prediction of the Phase Diagram of DNA-Functionalized Nanosized Colloids," *Physical Review Letters,* 2012. 108(26).

[25] R. e. a. Jin, "What controls the melting properties of DNA-linked gold nanoparticle assemblies?," *Journal of the American Chemical Society,* pp. p. 1643-1654, 2003. 125(6).

[26] J. Anne-Laure M. Le Ny and C. Ted Lee, "Photoreversible DNA Condensation Using Light-Responsive Surfactants," *J. Am. Chem. Soc.,* p. p 6400–6408, 2006, 128 (19).

[27] C. C. A. D. T. H. H. S. K. Y. D. B. A. Estévez-Torres, "Sequence-independent and reversible photocontrol of transcription/expression systems using a photosensitive nucleic acid binder," *Proc. Natl. Acad. Sci. USA,* 2009 106.

[28] S. T. T. a. P. D. Torquato, "Is random close packing of spheres well defined?," *Physical Review Letters,* pp. p. 2064-2067, 2000. 84(10).

[29] K. J. M. B. a. B. A. G. Rafal Klajn, "Light-controlled self-assembly of reversible and," *PNAS,* pp. p.

10305-10309, (2007) 104.25.